

Polymer Ligands with Quaternary Ammonium Binding Motifs on Metal Nanoparticles Enable Selective Ion Transport for CO₂ Electroreduction

Debasmita Muhuri,^[a] Manthan Sarkar,^[a] Hanyi Duan,^[b] Lindsey A. Hanson,^[c] Jie He,^{[a],[b],*}

[a] D. Muhuri, M. Sarkar, Prof. J. He
Department of Chemistry University of Connecticut, Storrs, Connecticut 06269, USA
E-mail: jie.he@uconn.edu

[b] Dr. H. Duan, Prof. J. He
Polymer Program, Institute of Materials Science, University of Connecticut, Storrs, Connecticut 06269, USA

[c] Prof. L. Hanson
Department of Chemistry, Trinity College, Hartford, Connecticut 06106, USA

Supporting information for this article is given via a link at the end of the document. Ligand synthesis and exchange methods, and more results on electron microscopy, spectroscopy, catalysis are available in supporting information.

Abstract: We report a new class of hydrophobic polymer ligands with quaternary ammonium head groups for surface modification of noble metal nanoparticles (NPs). Quaternary ammonium ligands bind NPs through non-covalent electrostatic interactions, producing polymer-grafted NPs with high colloidal and chemical stability. These polymers having charged head groups offer powerful strategies to tailor the structure and function of metal-electrolyte interfaces in electrocatalytic systems. The ammonium head groups serve as ionic reservoirs that preconcentrate bicarbonate counterions at the surface of nanocatalysts, while the hydrophobic polymer backbones restructure local hydrogen-bonding networks, modulating water and ion transport dynamics. These interfacial effects promote CO₂ electroreduction, particularly under diffusion-limited conditions, resulting in a CO Faradaic efficiency (FE) exceeding 90%.

There has been significant interest in understanding how the surface characteristics of metal nanoparticles (NPs) influence their catalytic behavior, such as facet-dependent reactivity.^[1] On the other hand, organic ligands, as an important component on NP surfaces, have been treated traditionally as inert stabilizers, with little consideration given to their potential catalytic roles.^[2] More recently, growing attention has been directed toward organic ligands as active components that can modulate surface accessibility and shape the local solvation environment, collectively referred to as the microenvironment.^[3] This microenvironment can have a profound impact on both catalytic activity and selectivity. In particular, new functional groups and binding motifs of ligands have emerged as key factors in producing such an effect.^[4] In the case of CO₂ electroreduction, amine-containing ligands, including cysteamine,^[4f, 5] oleylamine,^[6] and pyridine,^[7] have been suggested to stabilize the reaction intermediate through hydrogen bonding both theoretically and experimentally. More recent studies on N-heterocyclic carbenes (NHCs) as strong σ donors have also suggested that changes in the electronic nature of metals can enhance the selectivity of CO₂ over proton reduction.^[8]

Polymeric ligands with extended coordination spheres can substantially impact the structure of metal-electrolyte interfaces. A prominent example from the Sargent group demonstrated that coating Cu catalysts with perfluorinated sulfonic acid (PFSA) ionomers enabled highly selective CO₂ reduction, achieving over 90% total Faradaic efficiency, with 65–75% directed toward C₂H₄.^[9] Our group has shown that brush-like polymer ligands exhibit distinct interfacial behavior,^[8b, 10] compared to molecular self-assembled monolayers (SAMs) that often act as insulating layers for ions and electrons.^[11] Notably, hydrophobic or zwitterionic ligands can strongly influence the local hydrogen-bonding network of water, thereby modulating mass transport processes relevant to electrolysis. In the current study, we designed hydrophobic polymer ligands containing quaternary ammonium head groups for functionalizing noble metal NPs. We demonstrate that cationic binding motifs within these polymers modulate ion transport and restructure the interfacial environment. During CO₂ electroreduction, these positively charged polymer shells acting as ion reservoirs,^[12] remained tightly bound to negatively polarized electrodes, attracting and

COMMUNICATION

preconcentrating bicarbonate counterions to the catalyst interface. This localized accumulation of bicarbonate promotes CO₂ reduction, especially under diffusion-limited conditions.^[13]

Quaternary ammonium groups which have long been used for controlled growth and stabilization of noble metal NPs^[14] have not yet been previously reported on polymer ligands. The ammonium binding motifs were introduced via alkylation of halogen-terminated polystyrene (PS) synthesized through atom transfer radical polymerization (ATRP) using ethyl α -bromoisobutyrate (EBIB) as an initiator. Three different amines, including trimethylamine (TMA), N,N,N',N'-tetramethylethylenediamine (TEMEDA), and N,N,N',N'',N''-pentamethyldiethylenetriamine (PMDETA), were used to generate polymer ligands with varying quaternary ammonium content (see SI for synthetic details). The parent polymer PS₂₃₅-Br has a number-average molecular weight (M_n) of 24.6 kg/mol and a polydispersity index (PDI) of 1.09, measured on a gel permeation chromatography (GPC) calibrated with PS standards. P1-P3 were synthesized from PS₂₃₅-Br using three different types of amines, i.e., monodentate P1 with TMA, bidentate P2 with TEMEDA, and tridentate P3 with PMDETA (Figure 1a). For P2 and P3, further quaternization of their tertiary amines was carried out with iodomethane (CH₃I), see SI for synthetic details). The quaternization was characterized by ¹H NMR. The methyl and methylene groups on ammonium appeared as a broad peak in the range of 3.2 to 4.0 ppm. For P2, the conversion was calculated to be 83%, using aromatic protons as an internal standard. Incomplete conversion is likely attributed to the strong repulsion between the two positively charged N atoms at a close distance. After quaternization, P2 has an M_n of 24.8 kg/mol and a PDI of 1.11 (Figure S1). In infrared spectroscopy (Figure S1c), P0 and P2 display characteristic stretching frequencies around 2960 cm⁻¹, corresponding to C-H stretching. A weak new peak appeared at 1100 cm⁻¹ for P2, indicating the formation of C-N bonds.

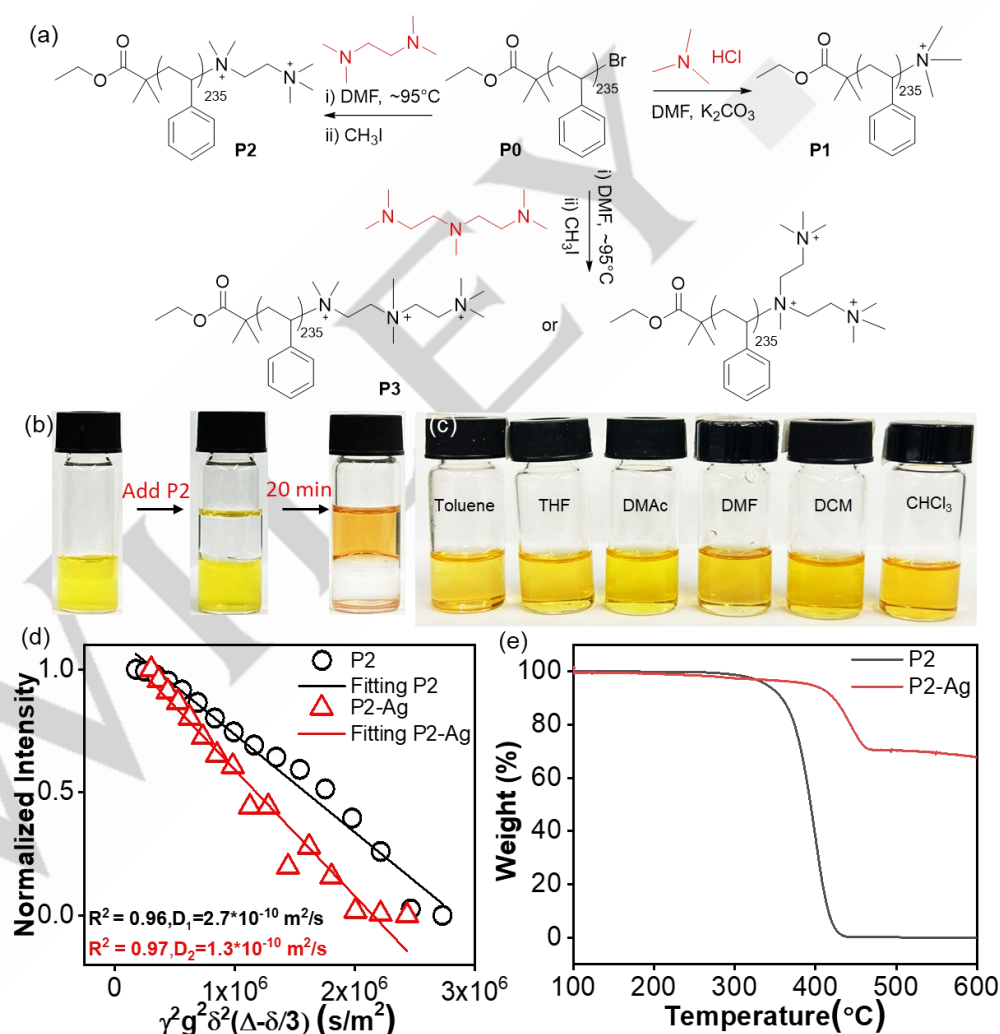


Figure 1. (a) Synthesis of the parent polymer P0 and quaternary ammonium-containing polymer ligands P1-P3 using three different amines, i.e., TMA, TEMEDA, and PMDETA, respectively. (b) Modification of AgNPs using P2 at the interface of water/toluene. (c) P2-modified AgNPs in different organic solvents: toluene, tetrahydrofuran (THF), dimethylacetamide (DMAc), dimethylformamide (DMF), dichloromethane (DCM), chloroform (CHCl₃). (d) DOSY-NMR attenuation curve fitting for P2 (black) and P2-modified AgNPs (red) where Δ is diffusion time, δ is

COMMUNICATION

pulse length, γ is proton gyromagnetic ratio, g is gradient strength and D_1 , D_2 are diffusion coefficients of P2 and P2-modified AgNPs respectively. (e) TGA curves for P2 (black) and P2-modified AgNPs (red), respectively.

The ligand exchange of citrate-capped metal NPs with P2 was carried out through phase transfer.^[15] Typically, the aqueous solution of silver NP (AgNP, ~29 nm, 0.5 mg/mL) was mixed with P2 (0.2 mg/mL) dissolved in toluene at equivalent volume. The resulting mixture was vortexed for 20 min (Figure 1b). The phase transfer of AgNPs occurred as indicated by the color switch of water and toluene phases. The toluene phase was collected and centrifuged three times at 8000 rpm for 20 min. The resulting precipitate could be well dispersed in a range of organic solvents that are good solvents for PS (Figure 1c). UV-vis spectroscopy was used to assess the stability of P2-modified AgNPs. AgNPs had the localized surface plasmon resonance (LSPR, Figure S2a) band at 410 nm in water. After modification by P2, AgNPs also showed well-resolved LSPR peaks in various organic solvents, confirming their colloidal stability across different solvents. There was also a clear redshift of 10–15 nm, arising from the change in refractive index of different solvent media. Transmission electron microscopy (TEM) reveals that AgNPs retained their structural integrity, with an average diameter of approximately 29 nm before and after surface modification (Figure S2b-c). This phase transfer method can be scaled up to >200 mL of AgNPs (Figure S2d). P3 having an M_n of 25.6 kg/mol and a PDI of 1.11 (Figure S3) as the tridentate ligand could also modify AgNPs similarly (Figure S4a). However, P1 having an M_n of 23.2 kg/mol and a PDI of 1.09 (Figure S3) with a monodentate ammonium binding motif did not transfer AgNPs within 2 h (Figure S4). The molecular weight of PS seems to be less important for ligand exchange. We examined bidentate ammonium-containing PS₂₅ (P2-L) with a M_n of 2.5 kg/mol (Figure S5) that modified AgNPs similarly (Figure S6). Quaternary ammonium-terminated polyethylene glycol (PEG, M_n of 2.0 kg/mol) (Figure S7) also modified AgNPs at the interface of chloroform and water (Figure S8).

Surface modification of AgNPs by P2 was confirmed by ¹H NMR spectroscopy and diffusion-ordered spectroscopy (DOSY). ¹H NMR spectra of both free P2 and P2-functionalized AgNPs exhibited similar chemical shifts for the PS backbone and aromatic protons, indicating the presence of P2 on AgNPs (Figure S9a). Their diffusion behaviours had a clear difference (Figure 1d). DOSY analysis revealed a single diffusion coefficient (D_0) of 2.7×10^{-10} m²/s for free P2. Upon grafting to AgNPs, the diffusion coefficient decreased to 1.3×10^{-10} m²/s, consistent with reduced mobility due to surface confinement of the polymer chains. The corresponding hydrodynamic radius was doubled for P2-grafted AgNPs, suggesting the formation of an extended polymer layer on the AgNP surface. The grafting density was estimated using thermogravimetric analysis (TGA, Figure 1e). The density of P2 on AgNPs was approximately 0.52 chains/nm² (See SI for details), comparable to the reported values for thiol-terminated polymers.^[16] Infrared and Raman spectroscopy further confirmed surface functionalization. Both free and grafted P2 exhibited characteristic C–H stretching vibrations near 3200 cm⁻¹ (aromatic) and 2960 cm⁻¹ (alkyl). Notably, Raman spectra showed a pronounced enhancement of the aromatic C–H band upon grafting, indicative of strong surface interactions with AgNPs (Figure S9b-d).

Moreover, we titrated the THF solution of P2-grafted AgNPs with water as a non-solvent for PS to confirm the surface hydrophobicity. With the gradual increase of water, the collapse of PS chains resulted in the aggregation of AgNPs (Figure S10). Under UV-vis, a noticeable redshift of the Ag LSPR was observed. The critical water concentration (C_{CWC}) defined by the sharp shift of the LSPR peak was approximately 18.7% relative to THF, close to that observed in thiol-terminated PS-grafted AuNPs.^[17]

AgNPs with quaternary ammonium-terminated polymer ligands showed high colloidal stability against oxidation. Hydrogen peroxide (H₂O₂), as a strong oxidant, can etch AgNPs.^[15a] Citrate-capped AgNPs would be readily dissolved stoichiometrically upon titrating with H₂O₂ (~30 wt %) at less than 1 vol% (Figure 2a-b). P2-modified AgNPs were stable up to 10 vol% of H₂O₂ solution. A similar trend was observed with organic oxidants, e.g., tert-butyl hydroperoxide (TBHP, Figure 2e-f). P2-modified AgNPs were stable up to 50% of TBHP in THF, while citrate-capped AgNPs showed fast dissolution. These results highlight enhanced oxidative stability imparted by P2, likely stabilizing the surface Ag⁺ species without leaching. Similarly, P2-modified AgNPs showed high stability against oxidative etching of cyanide (CN⁻) (Figure S11). We also examined competitive ligands, e.g., 3-mercaptopropionic acid (3-MPA, Figure 2c-d). Molecular thiols showed fast binding with AgNPs and caused the aggregation of AgNPs even at 1 μ L. P2-modified AgNPs were stable in THF containing 3-MPA up to 5 vol% in THF. Those results suggested that quaternary ammonium binds with Ag dynamically as it is replaceable by thiols. As our control, when ligand exchange with PEG₁₁₄-SH was carried out in THF, hydrophobic P2-modified AgNPs could be transferred to water (Figure S12). Previous studies on crystallography of metal nanoclusters^[18] or spectroscopy with plasmonic NPs,^[19] suggested that quaternary ammonium binds with metal NPs with electrostatic interactions where halide ions bridge the surface metal atoms and positively charged ammonium. We did not observe that counterions (Br⁻ and I⁻) of quaternary ammonium played an important role in ligand exchange of those NPs, although halides as counter ions are present in the synthesis of all NPs.

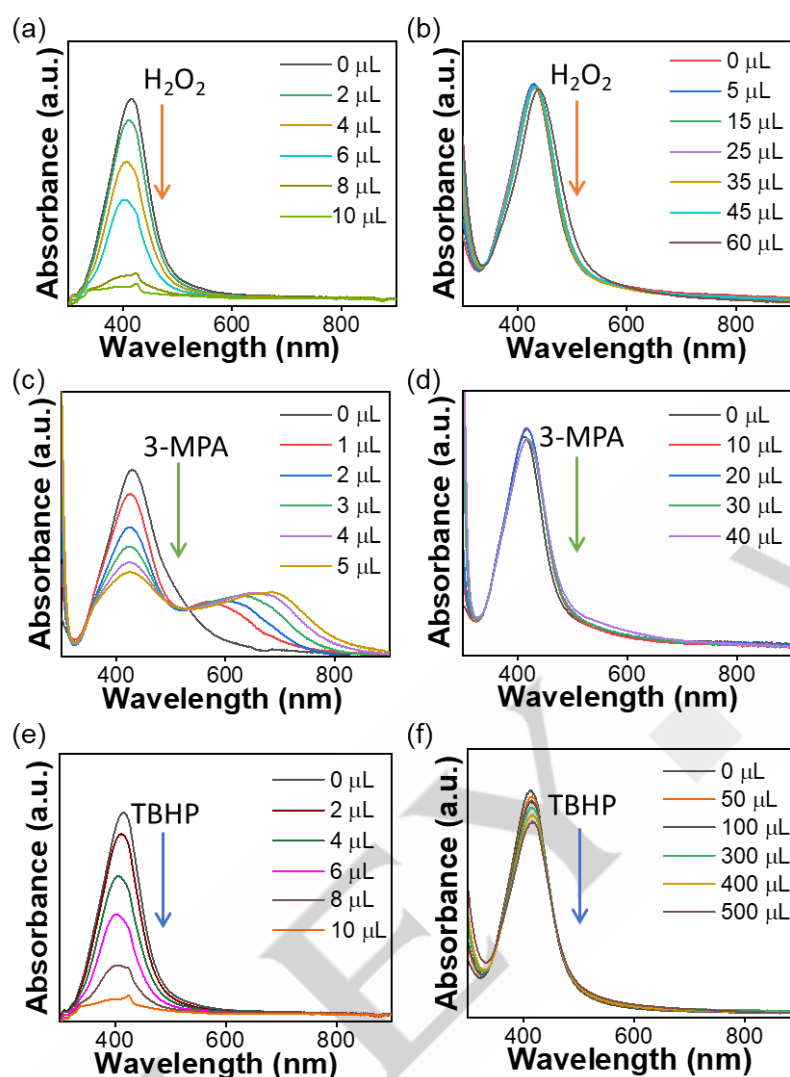


Figure 2. UV-vis spectra showing the oxidative stability (a,c,e) pristine AgNPs and (b,d,f) P2-modified AgNPs upon addition of hydrogen peroxide (H_2O_2 , 30 wt %), 3-mercaptopropionic acid (3-MPA, 100 mM) and *tert*-butyl hydroperoxide (TBHP, 100 mM), respectively.

Quaternary ammonium-terminated polymers can also modify other metal NPs, including Au, Pd, and Pt, with different sizes and shapes. In examples of nanospheres of Au (Figure S13), Pd (Figure S14a), and Pt (Figure S14b), similar phase transfer from the aqueous to toluene phase containing P2 was observed. After purification, P2-modified AuNPs formed stable a colloidal suspension in various organic solvents that are good solvents for PS. Similarly, quaternary ammonium-terminated polymers can replace cetyltrimethylammonium chloride (CTAC) or cetyltrimethylammonium bromide (CTAB) as capping agents broadly used in NP synthesis (see SI Section 3). As examples, ligand exchange of CTAC-capped AuNPs and CTAB-capped Au nanorods with P2 could be carried out in THF (Figure S14c-d).

We further assessed the impact of quaternary ammonium-terminated polymers on the catalyst-electrolyte interface. As an example, AuNPs modified by P2 (P2-AuNPs) were studied for CO_2 electroreduction. AuNPs were modified with P2 after being loaded on carbon nanospheres (~50 nm in diameter, see SI for details, Figure S15). Cyclic voltammetry (CV) was first conducted in 0.5 M H_2SO_4 under N_2 to determine the electrochemically active surface area (ECSA). In the cathodic scan, a characteristic reduction peak of Au was observed at ca. 1.1 V vs. reversible hydrogen electrode (RHE), arising from the reduction of surface oxygenated monolayer (Figure 3a). Using the peak area from CV, the ECSA of P2-AuNPs was determined to be $0.146 \text{ cm}^2 \text{ mg}^{-1} \text{ Au}$, compared to that of pristine AuNPs, $0.154 \text{ cm}^2 \text{ mg}^{-1} \text{ Au}$. This suggests that the presence of polymer ligands did not block surface accessibility at a relatively low grafting density, different from molecular SAMs.^[11] Quaternary ammonium with its dynamic non-covalent interaction^{[20][21]} likely allows access to the surface site, as compared to thiol- or carbene-

COMMUNICATION

ended polymer ligands.^[15b, 22] The catalytic CO₂ electroreduction was examined first by linear sweep voltammetry (LSV) in 0.1 M KHCO₃ under saturated CO₂ (Figure 3b). P2-AuNPs had a higher catalytic current, as compared to unmodified Au/C. At -1.0 V vs. RHE, the catalytic current J , normalized by their ECSA, is -23.4 and -9.7 mA cm⁻² for P2-AuNPs and Au/C, respectively. In the potential range of -0.6 to -1.5 V, P2-AuNPs showed roughly 3 times higher current density than that of pristine Au/C. In steady-state chronoamperometric measurements ($i-t$), the current of P2-AuNPs and Au/C can also be compared to examine their activity at different potentials (Figure S16). P2-AuNPs also had a higher catalytic current across all tested potentials. At -1.2 V vs. RHE, the steady-state current for P2-AuNPs is -7 mA, about two times higher than that of Au. These results confirmed the favorable CO₂ reduction kinetics in the presence of quaternary ammonium-terminated polymers.

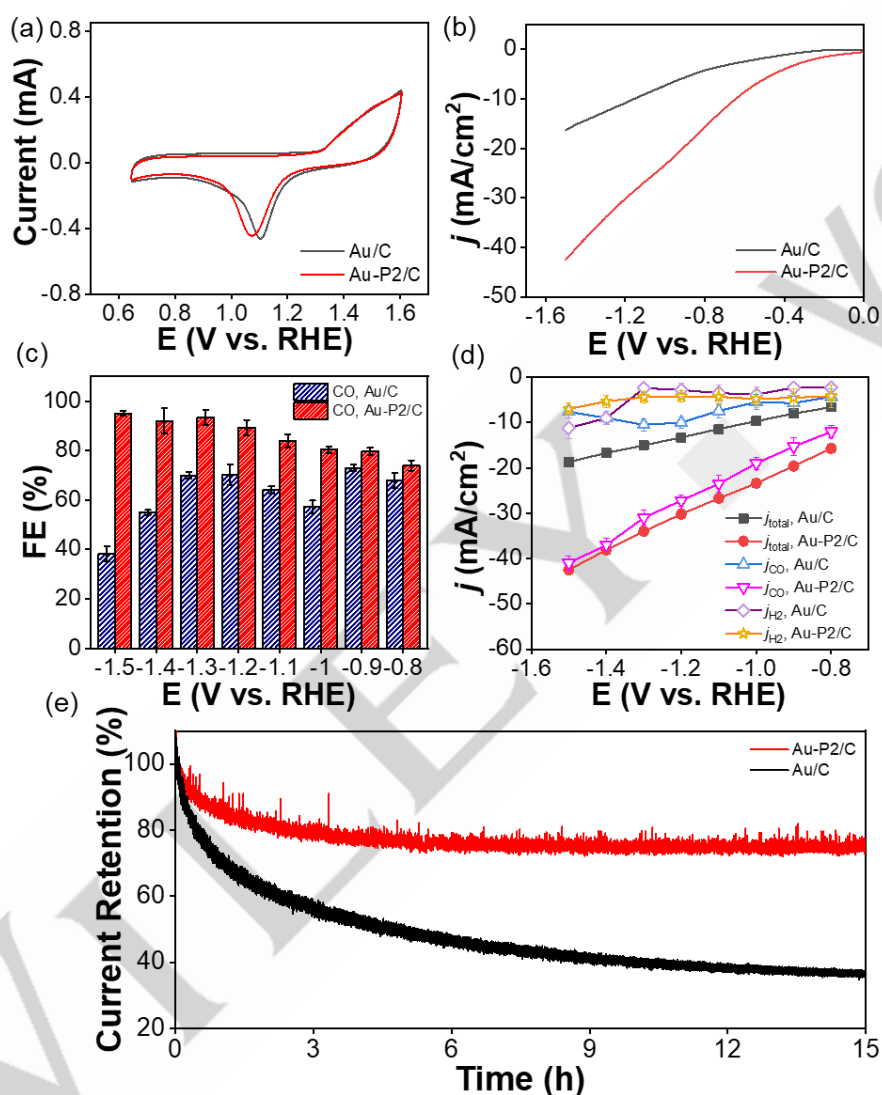


Figure 3. Electrochemical studies of P2-modified AuNPs. (a) CVs measured under N₂ saturated 0.5 M H₂SO₄ at 100 mV s⁻¹. (b) LSVs measured under CO₂-saturated 0.1 M KHCO₃ at 100 mV s⁻¹. The current density (j) is relative to the ECSA of AuNPs. (c) Faradaic efficiency (FE) of CO at different potentials for CO₂ reduction of Au/C and Au-P2/C under CO₂-saturated 0.1 M KHCO₃. The standard deviation of FE was determined from three independent measurements. (d) Partial current density analysis for CO production (j_{CO}) and H₂ production (j_{H_2}). (e) Chronoamperometric measurements showing the current retention (%) at -0.9 V for 15 h of Au-P2/C and Au/C.

Analysis of CO₂ electroreduction was carried out in an H-cell separated with a proton exchange membrane using 0.1 M KHCO₃ as a supporting electrolyte. CO₂ reduction with Au/C without P2 had a CO faradaic efficiency (FE) of 50%-70% in the potential range of -0.8 V to -1.3 V (Figure 3c), in good agreement with the reported values in literature.^[3f, 23] Note that CO FE dropped rapidly at a potential below -1.3 V.^[24] At -1.5 V, the CO FE of Au/C decreased to ca. 40%, suggesting that the diffusion-controlled reaction (limited by CO₂ concentration) is dominated by proton reduction at a higher current density. With P2, the CO FE improved clearly across all potential ranges. Surprisingly, P2-AuNPs became more selective at a lower potential. The CO FE remained to be >94% at potential -1.5 V (Figure 3c and Table S1-S2). Quantitatively, the partial current density toward CO formation (J_{CO}) for P2-

COMMUNICATION

AuNPs showed a continuous increase when lowering the reduction potential (Figure 3d). The J_{CO} reached -41 mA cm^{-2} at -1.5 V , while the partial current density for H_2 (J_{H_2}) remained largely unchanged, about -7 mA cm^{-2} . As a comparison, the J_{CO} of Au/C started to decrease below -1.3 V . At -1.5 V , the J_{CO} of Au/C decreased to -7.6 mA cm^{-2} , about 19% of that on P2-AuNPs (Figure 3d). These results suggest that quaternary ammonium-terminated polymer ligands somehow improved the local concentration of CO_2 (as the increase of kinetic current for CO) under more negative bias, likely contributing to the high selectivity for CO_2 over proton reduction. The long-term stability of P2-AuNPs and pristine Au/C are assessed by chronoamperometric $I-t$ measurements at -0.9 V over 15 h. Au-P2/C showed approximately 75% of current retention, whereas Au/C without polymers lost $>65\%$ of its initial activity (Figure 3e).

To gain mechanistic insights, we used attenuated total reflectance-surface-enhanced infrared absorption spectroscopy (ATR-SEIRAS) to monitor the ligand-electrolyte interface under reaction conditions. The SEIRAS spectra (background subtracted under no bias) were collected while applying a linear sweep from 0 V to -2 V at a scan rate of 100 mV s^{-1} (Figure 4a). Under reductive potentials, a broad peak at 3450 cm^{-1} assigned to O-H stretching from water was seen. Its peak intensity increased with negative bias. The upward peak indicated the surface adsorption of water molecules. This has been previously observed by others and our group.^[10b, 25] The dipole interaction of water on negatively charged electrode is likely aligned in the H-down position. In the absence of polymer ligands, the broad O-H stretching peak also suggests the coexistence of mixed free water and clustered water with hydrogen bonding.^[8b, 10b]

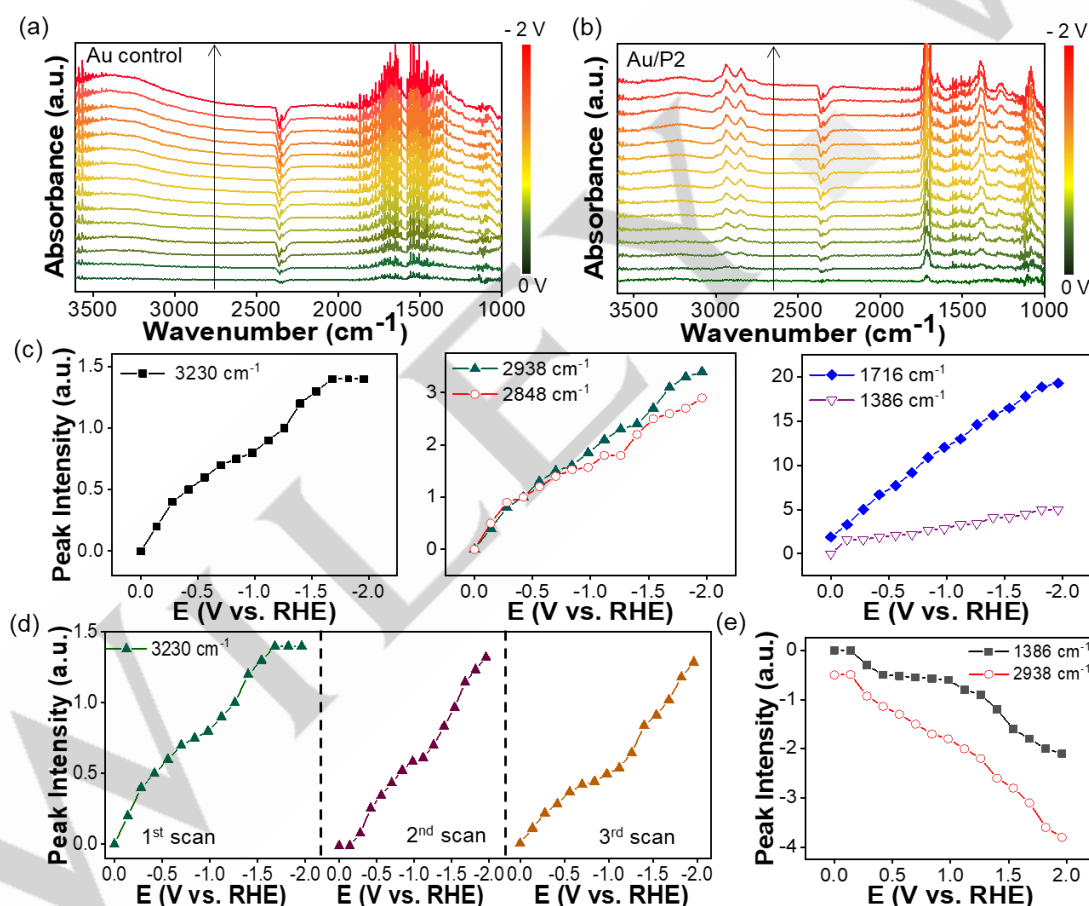


Figure 4. Electrochemical infrared spectroscopic studies of Au with P2. *In situ* ATR-SEIRAS spectra of (a) Au control and (b) P2-modified Au within the range of 0 V to -2 V with an interval of about -134 mV . Vibrational peak intensity changes of P2-modified Au at (c) 3230 cm^{-1} , 2938 cm^{-1} , 2848 cm^{-1} , 1716 cm^{-1} , and 1386 cm^{-1} , and (d) at 3230 cm^{-1} for three scans from 0 to -2 V . (e) Vibrational peak intensity of P2-modified Au at 1386 cm^{-1} and 2938 cm^{-1} when scanned from 0 to 2 V .

With P2, the O-H stretching of water showed a clear peak at 3230 cm^{-1} under negative bias, about 220 cm^{-1} redshifted as compared to that without polymer (Figure 4b). This shift is assigned to the formation of water clusters with strong hydrogen bonding network where the local hydrophobicity of polymer ligands likely promotes the clustering of water.^[26] Using the two spectra at -2.0 V , we further analyzed the hydrogen bonding of water through

COMMUNICATION

peak deconvolution (Figure S17). For Au control, the two best-fitting peaks at 3469 cm^{-1} (59%) and 3222 cm^{-1} (41%), are assigned to weakly H-bonded water and strongly H-bonded water, respectively, similar to that of liquid water. Au-P2 can also be fitted as a mixture of weakly H-bonded and strongly H-bonded water, appearing at 3416 cm^{-1} and 3230 cm^{-1} , respectively. However, the strongly H-bonded water accounts for approximately 92%. Those results suggest that water molecules have a dense hydrogen bonding network presumably because of the hydrophobic microenvironment created by P2. This largely contributed to the suppression of hydrogen evolution reactions (HERs) as reported earlier.^[8b, 10b, 27]

New peaks appearing at 2938 cm^{-1} and 2848 cm^{-1} were assigned to C–H stretching from the backbone of P2. With a cathodic sweep from 0 V to -2 V, we observed that the two peaks became more pronounced as upward peaks at a lower potential (Figure 4c). We cycled the linear sweep from 0 V to -2 V three times, and such peak enhancement was reproducible (Figures 4d and S18). We attributed this change to the progressive accumulation of P2 at the near surface under reductive potentials, because of electrostatic attraction. To confirm whether polymers are electrostatically attracted to the electrode, we carried out control experiments using an anodic scan from 0 V to 2 V (Figures 4e and S18). The C–H stretching peaks showed a downward trend with continuous decrease in peak intensity. Since no free polymer ligands are present in solution, the peak intensity change is attributed to the distance change of polymer ligands to the Au electrode.

Along with the change of the C–H stretching, there were other peaks for Au modified with P2 at 1716 cm^{-1} and 1386 cm^{-1} , assigning to O–H bending and symmetric stretching peak of hydrated bicarbonate, respectively.^[28] Those two peaks also showed an upward trend when lowering the potential. Two other new peaks between 1000 cm^{-1} and 1200 cm^{-1} having a similar upward trend are likely from the hydration clusters of bicarbonate as reported previously.^[28a] At -2 V, the peak intensity of bicarbonate had a significant enhancement as compared to that at 0 V. Although bicarbonates are not favored at negatively charged surfaces (not observed in the Au control),^[28b] their accumulation is attributed to local charge compensation. As the cationic ammonium of P2 approaches the catalyst, bicarbonate counterions are drawn into the interfacial region to maintain local electroneutrality. This behavior was consistent across three independent scan cycles (Figure S18), demonstrating the reproducibility of these potential-induced spectral features. The preconcentration of bicarbonate likely maintains the CO_2 concentration near the electrode surface.^[28b] Therefore, quaternary ammonium-functionalized ligands significantly reshape the ligand–electrolyte interface by preconcentrating counterions. Together with the hydrophobic microenvironment provided by polymer ligands that restructures interfacial water, these ammonium-containing polymers significantly impact local water/ CO_2 transport and availability, thereby improving CO_2 reduction selectivity.

To summarize, we demonstrated the use of quaternary ammonium-containing polymers as surface ligands for noble metal NPs. Polymers having bidentate quaternary ammonium head groups were able to bind with a variety of noble metal NPs through non-covalent, electrostatic interactions. These polymer-grafted NPs exhibited high colloidal and chemical stability. The positively charged head group had a profound impact on the transport of ions and water at the catalyst–electrolyte interface. Under negative bias, bicarbonates as counterions were preconcentrated, while extended hydrophobic polymers modulated the hydrogen bonding network among water. The increased local concentration of bicarbonates potentially improved the selectivity of CO_2 to CO with a high CO FE exceeding 90% even under diffusion-limited conditions. These results highlight the critical role of polymer ligands to engineer microenvironments of nanocatalysts in uniquely controlling and gating reaction species.

Supporting Information

Ligand synthesis and ligand exchange methods, and more results on electron microscopy, spectroscopy, catalysis are available in supporting information.

Acknowledgments

The authors thank financial support from the National Science Foundation (CBET 2324346). The TEM images were obtained at the Biosciences Electron Microscopy Facility at the University of Connecticut. The Bruker Avance III used for NMR measurements was obtained with a National Science Foundation MRI grant (NSF-MRI CHE-0619275).

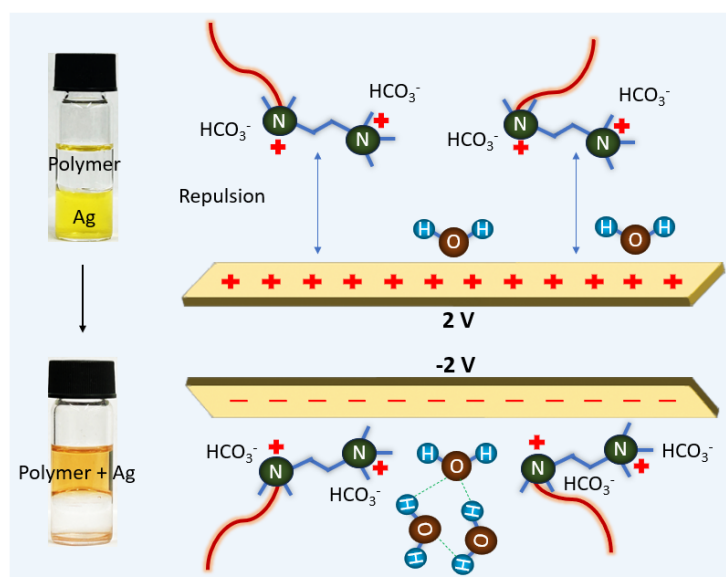
Keywords: ammonium ligands • polymer ligands • hydrophobicity • ion transport • CO_2 reduction

References

- [1] a) Q. Zhang, H. Wang, *ACS Catalysis* **2014**, *4*, 4027-4033;
b) F. Vines, J. R. Gomes, F. Illas, *Chemical Society Reviews* **2014**, *43*, 4922-4939;
c) D. Gao, H. Zhou, J. Wang, S. Miao, F. Yang, G. Wang, J. Wang, X. Bao, *Journal of the American Chemical Society* **2015**, *137*, 4288-4291.
- [2] a) Z. Wei, J. He, **2023**, 375-400, Hairy Metal Nanoparticles for Catalysis: Polymer Ligand-Mediated Catalysis. In *Hairy Nanoparticles* (eds Z. Lin and Y. Liu). <https://doi.org/10.1002/9783527835874.ch10>; b) M. Jun, D. Kim, M. Kim, M. Kim, T. Kwon, K. Lee, *ACS Omega* **2022**, *7*, 42655-42663.
- [3] a) S. Yu, D. Kim, Z. Qi, S. Louisia, Y. Li, G. A. Somorjai, P. Yang, *Journal of the American Chemical Society* **2021**, *143*, 19919-19927;
b) H. Guan, C. Harris, S. Sun, *Accounts of chemical research* **2023**, *56*, 1591-1601;
c) M. C. Sau T., *Journal of the American Chemical Society* **2004**, *126*, 8648-8649;
d) D. Wakerley, S. Lamaison, F. Ozanam, N. Menguy, D. Mercier, P. Marcus, M. Fontecave, V. Mougel, *Nature Materials* **2019**, *18*, 1222-1227;
e) A. R. Riscoe, C. J. Wrasman, A. A. Herzing, A. S. Hoffman, A. Menon, A. Boubnov, M. Vargas, S. R. Bare, M. Cargnello, *Nature Catalysis* **2019**, *2*, 852-863;
f) Z. Cao, S. B. Zacate, X. Sun, J. Liu, E. M. Hale, W. P. Carson, S. B. Tyndall, J. Xu, X. Liu, X. Liu, C. Song, J. H. Luo, M. J. Cheng, X. Wen, W. Liu, *Angewante Chem Int Ed Engl* **2018**, *57*, 12675-12679;
g) L. Jin, B. Liu, S. Duay, J. He, *Catalysts* **2017**, *7*, 44.
- [4] a) Q. Zhu, C. J. Murphy, L. R. Baker, *Journal of the American Chemical Society* **2022**, *144*, 2829-2840;
b) L. Zhang, Z. Wei, M. Meng, G. Ung, J. He, *Journal of Materials Chemistry A* **2020**, *8*, 15900-15908;
c) C. Kim, H. S. Jeon, T. Eom, M. S. Jee, H. Kim, C. M. Friend, B. K. Min, Y. J. Hwang, *Journal of the American Chemical Society* **2015**, *137*, 13844-13850;
d) C. Costentin, J.-M. Savéant, C. Tard, *ACS Energy Letters* **2018**, *3*, 695-703;
e) Z. Wang, L. Wu, K. Sun, T. Chen, Z. Jiang, T. Cheng, W. A. Goddard, 3rd, *The journal of physical chemistry letters* **2018**, *9*, 3057-3061;
f) Z. Wang, K. Sun, C. Liang, L. Wu, Z. Niu, J. Gao, *ACS Applied Energy Materials* **2018**, *2*, 192-195;
g) K. S. Rawat, A. Mahata, I. Choudhuri, B. Pathak, *The Journal of Physical Chemistry C* **2016**, *120*, 8821-8831;
h) C. M. Crudden, J. H. Horton, Ebralidze, II, O. V. Zenkina, A. B. McLean, B. Drevniok, Z. She, H. B. Kraatz, N. J. Mosey, T. Seki, E. C. Keske, J. D. Leake, A. Rousina-Webb, G. Wu, *Nature Chemistry* **2014**, *6*, 409-414;
i) Y. Fang, J. C. Flake, *Journal of the American Chemical Society* **2017**, *139*, 3399-3405;
j) D. M. Seitz O., Aguirre-Tostado F.S., Wallace R., Chabal Y., *Journal of the American Chemical Society* **2009**, *131*, 18159-18167.
- [5] a) C. Kim, H. S. Jeon, T. Eom, M. S. Jee, H. Kim, C. M. Friend, B. K. Min, Y. J. Hwang, *Journal of the American Chemical Society* **2015**, *137*, 13844-13850;
b) Z. Wang, L. Wu, K. Sun, T. Chen, Z. Jiang, T. Cheng, W. A. Goddard Iii, *The journal of Physical Chemistry Letters* **2018**, *9*, 3057-3061.
- [6] a) M. Gao, Y. Zhu, Y. Liu, K. Wu, H. Lu, S. Tang, C. Liu, H. Yue, B. Liang, J. Yan, *Chemical Communications* **2020**, *56*, 7021-7024;
b) Y. Zhao, C. Wang, Y. Liu, D. R. MacFarlane, G. G. Wallace, *Advanced Energy Materials* **2018**, *8*, 1801400.
- [7] Y. Fang, J. C. Flake, *Journal of the American Chemical Society* **2017**, *139*, 3399-3405.
- [8] a) S. Bhattacharjee, A. Tripathi, R. Chatterjee, R. Thapa, T. E. Mueller, A. Bhaumik, *ACS Catalysis* **2024**, *14*, 718-727;
b) Y. Chen, K. Wei, H. Duan, H. Sun, Z. Yu, A. Zohaib, P. Zhu, J. He, S. Sun, *Journal of the American Chemical Society* **2025**, *147*, 14845-14855;
c) Z. Cao, D. Kim, D. Hong, Y. Yu, J. Xu, S. Lin, X. Wen, E. M. Nichols, K. Jeong, J. A. Reimer, P. Yang, C. J. Chang, *Journal of the American Chemical Society* **2016**, *138*, 8120-8125;
d) M. R. Narouz, K. M. Osten, P. J. Unsworth, R. W. Y. Man, K. Salorin, S. Takano, R. Tomihara, S. Kaappa, S. Malola, C. T. Dinh, J. D. Padmos, K. Ayoo, P. J. Garrett, M. Nambo, J. H. Horton, E. H. Sargent, H. Hakkinen, T. Tsukuda, C. M. Crudden, *Nature Chemistry* **2019**, *11*, 419-425.
- [9] a) D. C. De Arquer F., Ozden A., Wicks J., Mccallum C., Kirmani A., Nam D., Gabardo C., Seifitokaldani A., Wang X., Li Y., Li F., Edwards J., Richter L., Thorpe S., Sinton D., Sargent E., *Science* **2020**, *367*, 661-666;
b) M. Fang, X. Miao, Z. Huang, M. Wang, X. Feng, Z. Wang, Y. Zhu, L. Dai, L. Jiang, *Journal of the American Chemical Society* **2024**, *146*, 27060-27069.

- [10] a) W. Z. Zhang L., Thaneeru S., Meng M., Kruzyk M., Ung G., Liu B., He J., *Angewante Chemie International Edition* **2019**, *131*, 15981-15987;
b) Q. Luo, H. Duan, M. C. McLaughlin, K. Wei, J. Tapia, J. A. Adewuyi, S. Shuster, M. Liaqat, S. L. Suib, G. Ung, P. Bai, S. Sun, J. He, *Chemical science* **2023**, *14*, 9664-9677;
c) Q. Luo, J. Tapia, L. Zhou, C. H. Liu, M. Liaqat, H. Duan, Z. Yang, M. P. Nieh, T. Emrick, P. Bai, J. He, *Nanoscale* **2024**, *16*, 15558-15567.
- [11] a) Y. J. Fan F., Cai L., Price D., Dirk S., Kosynkin D., Yao Y., Rawlett A., Tour J., Bard A., *Journal of the American Chemical Society* **2002**, *124*, 5550-5560;
b) L. R. Boubour E., *Langmuir : the ACS Journal of Surfaces and Colloids* **2000**, *16*, 4222-4228;
c) L. R. Boubour E., *The Journal of Physical Chemistry B* **2000**, *104*, 9004-9010.
- [12] M. Fan, J. E. Huang, R. K. Miao, Y. Mao, P. Ou, F. Li, X.-Y. Li, Y. Cao, Z. Zhang, J. Zhang, Y. Yan, A. Ozden, W. Ni, Y. Wang, Y. Zhao, Z. Chen, B. Khatir, C. P. O'Brien, Y. Xu, Y. C. Xiao, G. I. N. Waterhouse, K. Golovin, Z. Wang, E. H. Sargent, D. Sinton, *Nature Catalysis* **2023**, *6*, 763-772.
- [13] a) J. S. Zeng, N. Corbin, K. Williams, K. Manthiram, *ACS Catalysis* **2020**, *10*, 4326-4336;
b) W. Deng, P. Zhang, B. Seger, J. Gong, *Nature communications* **2022**, *13*, 803.
- [14] a) X. Ye, Y. Gao, J. Chen, D. C. Reifsnnyder, C. Zheng, C. B. Murray, *Nano Letters* **2013**, *13*, 2163-2171;
b) J. Mosquera, D. Wang, S. Bals, L. M. Liz-Marzan, *Accounts of Chemical Research* **2023**, *56*, 1204-1212;
c) S. T. Murphy J., Gole A., Orendorff C., Gao J., Gou L., Hunyadi S., Li T., *Journal of Physical Chemistry B* **2005**, *109*, 13857-13870;
d) S. Han, R. Balasubramanian, *Langmuir : the ACS Journal of Surfaces and Colloids* **2014**, *30*, 9063-9070;
e) G. A. Murphy J., Humyadi S., Orendorff C., *Inorganic Chemistry* **2006**, *45*, 7544-7554.
- [15] a) Z. Wei, M. Kayceety, A. Price, K. Wei, Q. Luo, S. Thanneeru, S. Sun, J. He, *ACS Applied Materials & Interfaces* **2022**, *14*, 55227-55237;
b) S. Thanneeru, K. M. Ayers, M. Anuganti, L. Zhang, C. V. Kumar, G. Ung, J. He, *Journal of Materials Chemistry C* **2020**, *8*, 2280-2288;
- [16] H. Duan, Q. Luo, Z. Wei, Y. Lin, J. He, *ACS Macro Letters* **2021**, *10*, 786-790.
- [17] J. He, X. Huang, Y. C. Li, Y. Liu, T. Babu, M. A. Aronova, S. Wang, Z. Lu, X. Chen, Z. Nie, *Journal of the American Chemical Society* **2013**, *135*, 7974-7984.
- [18] a) L. Qiao, N. Pollard, R. D. Senanayake, Z. Yang, M. Kim, A. S. Ali, M. T. Hoang, N. Yao, Y. Han, R. Hernandez, A. Z. Clayborne, M. R. Jones, *Nature communications* **2023**, *14*, 4408;
b) Y. Song, Y. Li, M. Zhou, H. Li, T. Xu, C. Zhou, F. Ke, D. Huo, Y. Wan, J. Jie, W. W. Xu, M. Zhu, R. Jin, *Nature communications* **2022**, *13*, 1235.
- [19] M. Tebbe, C. Kuttner, M. Mannel, A. Fery, M. Chanana, *ACS Applied Materials & Interfaces* **2015**, *7*, 5984-5991.
- [20] a) K. Shi, D. Le, T. Panagiotakopoulos, T. S. Rahman, X. Feng, *ACS Catalysis* **2025**, *15*, 3647-3659;
b) K. Shi, J. Janisch, Z. Ren, Z. Meng, D. Israel, D. Le, W. E. Kaden, T. S. Rahman, X. Feng, *Journal of the American Chemical Society* **2025**, *147*, 23277-23285.
- [21] D. Badgurjar, M. Huynh, B. Masters, A. Wuttig, *Journal of the American Chemical Society* **2023**, *145*, 17734-17745.
- [22] J. Kang, Y. X. Wang, F. Peng, N. N. Zhang, Y. Xue, Y. Yang, E. Kumacheva, K. Liu, *Angewante Chemie International Edition Engl* **2022**, *61*, e202202405.
- [23] W. Zhu, R. Michalsky, O. Metin, H. Lv, S. Guo, C. J. Wright, X. Sun, A. A. Peterson, S. Sun, *Journal of the American Chemical Society* **2013**, *135*, 16833-16836.
- [24] B. A. Zhang, T. Ozel, J. S. Elias, C. Costentin, D. G. Nocera, *ACS Central Science* **2019**, *5*, 1097-1105.
- [25] a) E. R. Corson, R. Kas, R. Kostecki, J. J. Urban, W. A. Smith, B. D. McCloskey, R. Kortlever, *Journal of the American Chemical Society* **2020**, *142*, 11750-11762;
b) Z. Tao, A. J. Pearce, J. M. Mayer, H. Wang, *Journal of the American Chemical Society* **2022**, *144*, 8641-8648;
c) M. Papisizza, A. Cuesta, *ACS Catalysis* **2018**, *8*, 6345-6352.
- [26] N. L. Dominique, A. Chandran, I. M. Jensen, D. M. Jenkins, J. P. Camden, *Chemistry European Journal* **2024**, *30*, e202303681.
- [27] M. McKee, M. Kutter, Y. Wu, H. Williams, M. A. Vaudreuil, M. Carta, A. K. Yadav, H. Singh, J. F. Masson, D. Lentz, M. F. Kuhnel, N. Kornienko, *Nature Chemistry* **2025**, *17*, 92-100.
- [28] a) W. T. Garand E., Goebbert D., Bergmann R., Meijer G., Neumark D., Asmis K., *Journal of the American Chemical Society* **2010**, *132*, 849-856;
b) M. Dunwell, X. Yang, B. P. Setzler, J. Anibal, Y. Yan, B. Xu, *ACS Catalysis* **2018**, *8*, 3999-4008.

WILEY-VCH



Hydrophobic polymer ligands with positively charged head groups show a profound impact on the transport of ions and water at the catalyst-electrolyte interface. Under negative bias, bicarbonates as counterions are preconcentrated, while extended hydrophobic polymers modulate the hydrogen bonding network among water.